JOURNAL OF MATERIALS SCIENCE 28 (1993) 6000–6006

Microstructure of SiCp-reinforced A356 cast Al metal-matrix composite

JIN YAN, LI CHUNZHI, MI JIAWEI, YAN MINGGAO
Institute of Aeronautical Materials, Beijing 100095, China

The microstructure of SiCp-reinforced A356 cast Al metal-matrix composite (MMC) has been investigated by means of transmission electron microscopy and energy-dispersive X-ray analysis. It is found that the MMC contains β-SiC, $(\beta + \gamma_2)$SiC composite, eutectic Si, GP zones of Si sequence, a new J phase and the amorphous phase $Al_xSi_9Ca_2$. The γ_2-SiC is lath-like with a triclinic crystal structure having $a=0.308$ nm, $b=0.305$ nm, $c=1.262$ nm, $\alpha=93.8°$, $\beta=90.0°$, and $\gamma=60.0°$. The J phase is bulk-like with a C-face-centred orthorhombic crystal structure having $a=0.680$ nm, $b=1.170$ nm and $c=0.826$ nm.

1. Introduction

The SiCp-reinforced cast Al metal-matrix composite (MMC) has undergone extensive studies due to its promising advanced properties.

Two kinds of SiC have been described [1, 2]. α-SiC has a hexagonal structure with $a=0.3076$ nm, $c=0.5048$ nm. It has many variants with c varying from 0.5048 to 98.86 nm; one important variant is 6H-SiC with $a=b=0.3082$ nm, $c=1.512$ nm. β-SiC has an f.c.c. structure with $a=0.4357$ nm; Liu *et al.* [3] observed a kind of α, β-SiC composite in 6061 Al MMC. Nutt [4, 5] found one-dimensional structures in β-SiC; Zhou *et al.* [6, 7] studies the twins and stacking faults in β-SiC; Ning *et al.* [2] reported the existence of a special 6H α-SiC variant with [0 1 0] growth direction.

There are now five different opinions about the SiC–Al matrix interface: (a) the existence of SiO_2 thin layers [8]; (b) the existence of Al_4C_3 thin layers [9]; (c) the formation of an interaction zone due to the diffusion of Al into SiC [10]; (d) a good coherence between the SiC and Al matrix, but no existence of interaction zone [11]; and (e) the existence of a solute-rich layer [12].

Large quantities of eutectic Si have been observed in the A356 cast Al alloy. The eutectic Si has an f.c.c. structure with $a=0.5430$ nm. There are now some arguments [13–15] about the growth of eutectic Si and the orientation relationship between the matrix and eutectic Si.

Several kinds of constituent phase may exist in A356 cast Al alloy [16–18]. They are the $Al_{15}(Fe, Mn)_3Si_2$ phase (b.c.c. structure, $a=1.23$ nm), the $FeSiAl_5$ phase (monoclinic structure, $a=b=0.612$ nm, $c=4.15$ nm, $\gamma=91°$), the $FeMg_3Si_6Al_8$ phase (h.c.p. structure, $a=0.663$ nm, $c=0.794$ nm), and the $(Cr, Fe)_4Si_4Al_{13}$ phase (b.c.c. structure, $a=1.25$ nm).

According to its chemical composition, two sequences of precipitate may exist in the A356 Al alloy [19, 20]. The equilibrium phases of each sequence are the Mg_2Si phase (f.c.c. structure, $a=0.638$ nm) and Si (f.c.c. structure, $a=0.5430$ nm), respectively.

In the present paper, the microstructure of A356 cast Al MMC composite has been investigated by means of transmission electron microscopy and energy-dispersive X-ray analysis.

2. Experimental procedure

The experimental Al MMC was produced by the Duralcan company. Its chemical composition (wt %) was measured as 5.35 C, 11.4 Si, 0.33 Mg, 0.13 Ti and 0.11 Fe. The samples were prepared with a Gatan 600 dif ion-miller, on a cold stage cooled with liquid nitrogen. The accelerating voltage was 6 kV, with specimen current 70 μA and incident angle 13°.

The observation was performed on an H-800 transmission electron microscope. The device for energy-dispersive X-ray (EDX) analysis (STEM mode) was TN 5500 equipped with a diamond-window detector for ultra-light elements. The software for selected-area diffraction (SAD) pattern analysis was set up by Li and Yan [21].

3. Results and discussion

3.1. The SiC particulate

Fig. 1 shows the metallography of SiC particulates in the experimental material. The SiC has an irregular shape with a size of 5–12 μm. The particles distribute rather homogeneously. The volume fraction of SiC is measured as 16.7 %. The small particles around SiC are eutectic Si.

Fig. 2a is the bright-field (BF) image of β-SiC. Stacking faults appear to exist. Fig. 2b is the corresponding SAD pattern for the [1 1 1] zone. This conforms to the previous studies of Zhou *et al.* [6, 7].

Fig. 3a is the BF image of β-SiC (marked B) for its [0 1 1] zone. As shown in the picture, a large number

0022–2461

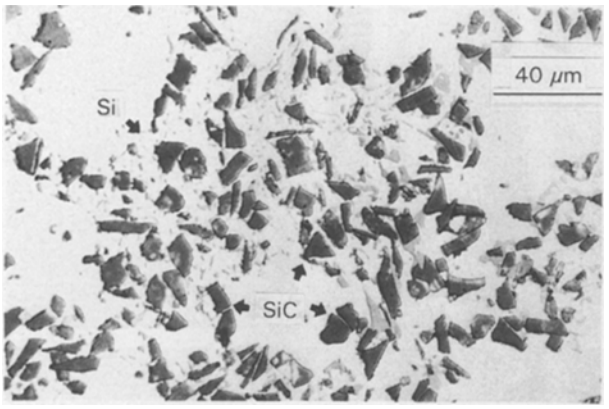

Figure 1 Metallography of SiC particulates and eutectic Si.

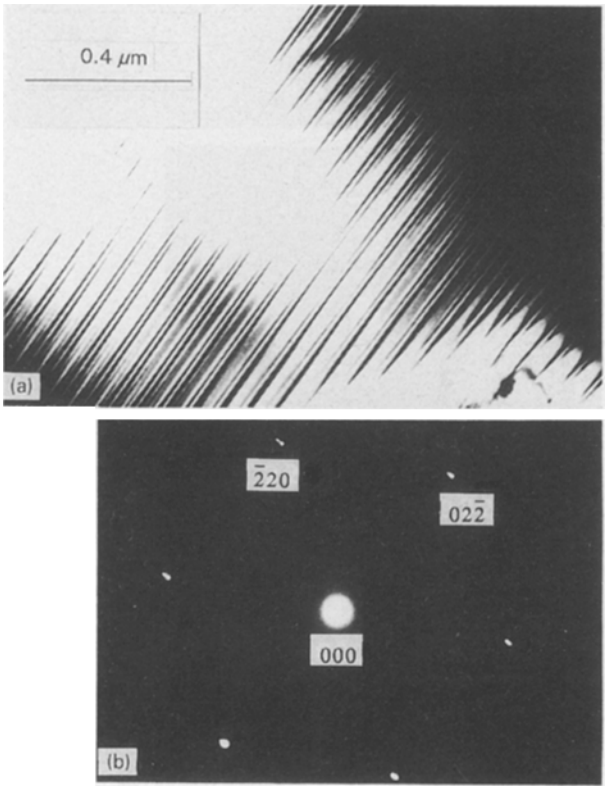

Figure 2 (a) Morphology of β-SiC and (b) the corresponding SAD pattern for the [1 1 1] zone.

TABLE I Measured values of SAD patterns in Fig. 3c to f

Fig. No.	R_2/R_1	θ(°)	d_1 (nm)
3c	1.13	92.0	0.229
3d	4.75	94.2	1.258
3e	12.50	89.0	1.258
3f	17.36	92.0	1.258

of lath-like phases (marked A) with sharply pointed heads (marked C) appear in the SiC. Fig. 3b is the corresponding dark-field (DF) image using the diffraction spot of the lath-like phase. Similar phenomena could also be observed in other images Fig. 3c to f are the SAD patterns of the lath-like phase. The larger diffraction spots in the patterns could be attributed to β-SiC and double diffraction between the β-SiC and lath-like phases. The measured values of these SAD patterns are shown in Table I. Here $\boldsymbol{R}_1$, $\boldsymbol{R}_2$ are the shortest and second shortest vectors of the two-dimensional reciprocal plane. d_1 is the plane spacing corresponding to $\boldsymbol{R}_1$, θ is the angle between $\boldsymbol{R}_1$ and $\boldsymbol{R}_2$. Fig. 3g is the SAD pattern of β-SiC for its [− 1 1 2] zone.

Since the group of SAD patterns in Fig. 3c to f could not be interpreted satisfactorily by any variants of SiC, including 6H-SiC, the authors have to believe that the lath-like phase in Fig. 3 is a new phase. It is determined that the lath-like phase has a triclinic crystal structure with $a = 0.308$ nm, $b = 0.305$ nm, $c = 1.262$ nm, $\alpha = 93.8°$, $\beta = 90.0°$ and $\gamma = 60.0°$. Table II shows the results of calculation which correspond to the experimental results of Table I. Here $(h_1\,k_1\,l_1)$ and $(h_2\,k_2\,l_2)$ are the planes corresponding to the two-dimensional reciprocal lattice vectors $\boldsymbol{R}_1$ and $\boldsymbol{R}_2$; $[U\,V\,W]$ is the direction of the reciprocal plane.

If the above structure of the lath-like phase is correct, the calculated inter-angles between the reciprocal planes in Table II should be consistent with the corresponding measured inter-angles between the SAD patterns in Fig. 3. This is another way to verify the structure of the lath-like phase when measurement errors cannot be avoided. The comparison is shown below, and the results are satisfactory.

Fig. 3c ^ Fig. 3d = 42.4° [4 2 − 1] ^ [1 0 0] = 42.93°

Fig. 3d ^ Fig. 3e = 23.0° [1 0 0] ^ [2 1 0] = 18.98°

Fig. 3e ^ Fig. 3f = 5.6° [2 1 0] ^ [3 1 0] = 5.18°

Fig. 3f ^ Fig. 3c = 37.0° [3 1 0] ^ [4 2 − 1] = 37.97°

Fig. 4 is a schematic diagram of the indexed patterns. Fig. 4a, b, c and d correspond to Fig. 3c, d, e and f, respectively.

Fig. 5 shows the result of energy-dispersive X-ray analysis of the SiC particulate in Fig. 3. Many spots have been detected. No significant difference of chemical composition between the lath-like phase and β-SiC was found. The appearance of a small Al peak could be attributed to the influence of the Al matrix.

Since the lath-like phase has a similar chemical composition but a different type of crystal structure to that of β-SiC, we would like to designate the phase as

TABLE II Calculated values of SAD patterns in Fig. 3c to f

Fig. No.	R_2/R_1	θ (°)	d_1 (nm)	$(h_1\,k_1\,l_1)$	$(h_2\,k_2\,l_2)$	$[U\,V\,W]$
3c	1.141	93.91	0.2336	0 1 2	1 0 4	4 2 − 1
3d	4.778	94.39	1.2583	0 0 1	0 − 1 0	1 0 0
3e	12.569	89.60	1.2583	0 0 1	1 − 2 1	2 1 0
3f	17.146	93.93	1.2583	0 0 1	1 − 3 1	3 1 0

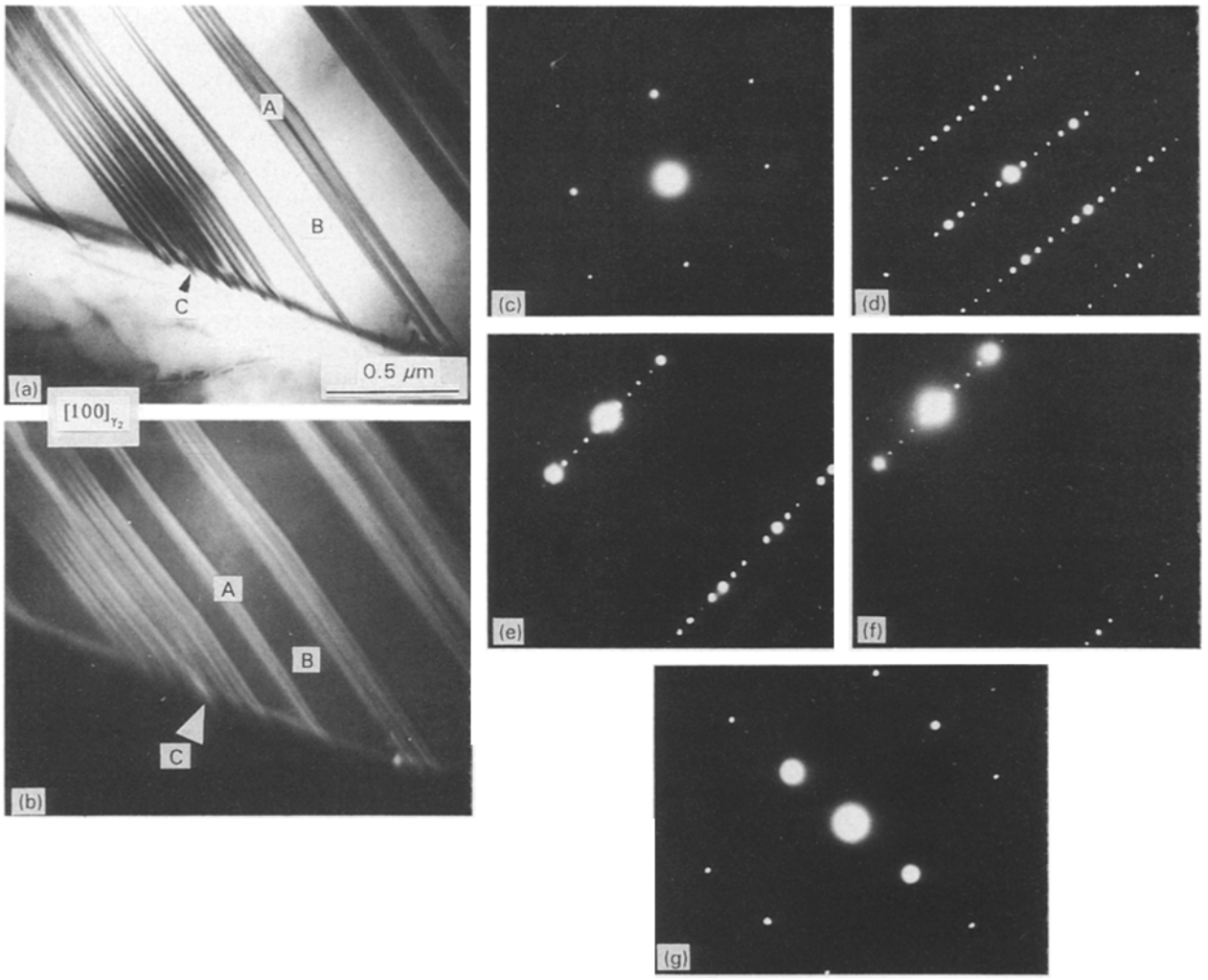

Figure 3 (a) Bright-field image of β and lath-like γ_2-SiC, (b) dark-field image of lath-like γ_2-SiC, (c–f) SAD patterns of lath-like γ_2-SiC, (g) SAD pattern of β-SiC for [1 1 2] zone.

γ_2-SiC phase. The formation mechanism of γ_2-SiC will be presented in another paper.

3.2. The interfacial structure between SiC particulate and Al matrix

Fig. 6 is the EDX spectrum obtained on the interface between the SiC particulate and the A1 matrix. The spot size of the electron beam was 100 nm. The spectrum indicates a localized segregation of carbon and yttrium. This result is quite different from previous views about the interfacial structure between the SiC and A1 matrix [8–12]. However, it may help to explain the rather homogeneous distribution of SiC in the MMC, because the rare-earth element Y may degrade the adhesion between the matrix and the SiC particulate.

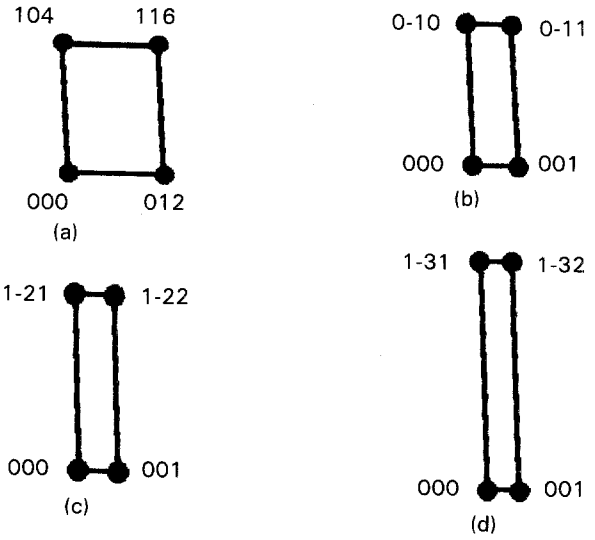

Figure 4 Indexed patterns corresponding to the SAD patterns of Fig. 3c to f.

3.3. The Si compounds

Fig. 7a and b are the respective BF and DF images of eutectic Si. There is a large quantity of stacking faults for the [1 1 1] direction. This is reasonable, since Si has a rather low stacking fault energy [22]. Fig. 8 shows the corresponding SAD patterns for [0 1 1], [1 1 2], [1 2 3] and [1 3 4] zones. No distinctive orientation relationships between the eutectic Si and Al matrix were evidenced. This result supports the view of Liu *et al.* [14].

Fig. 9 shows the morphology of the Al matrix and its SAD pattern for the [0 1 1] zone. A spherical

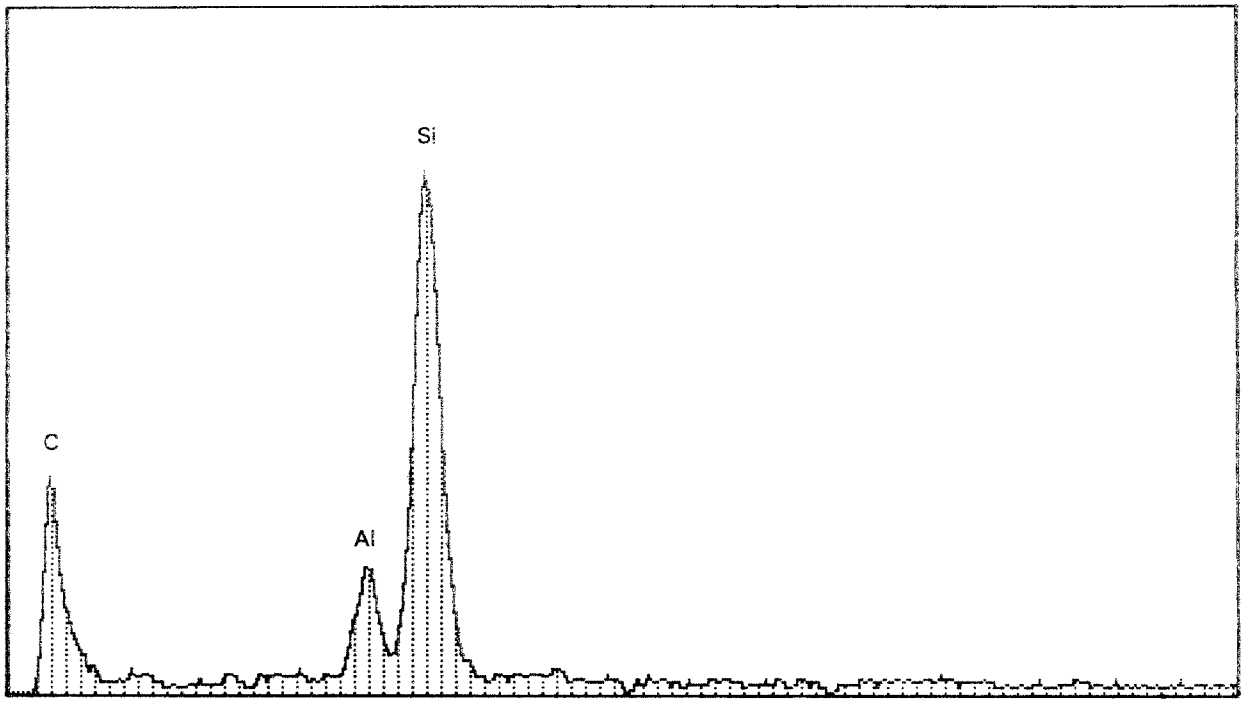

Figure 5 Energy-dispersive X-ray analysis of the SiC in Fig. 3.

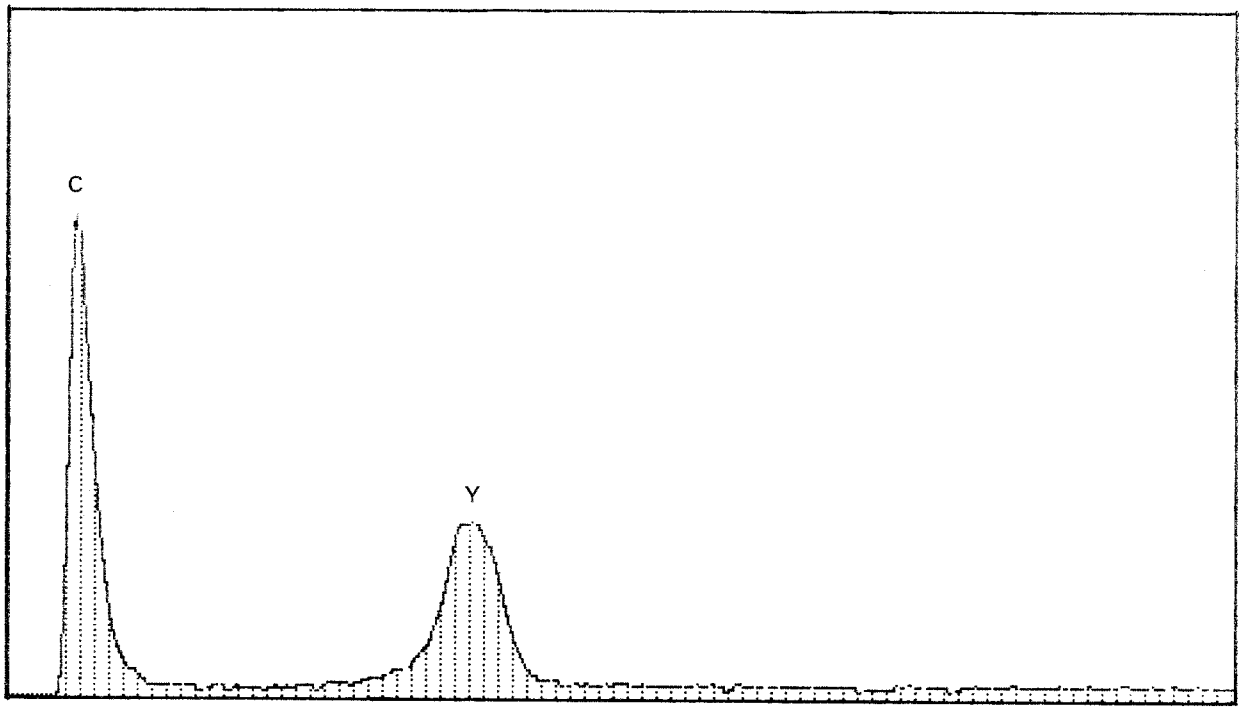

Figure 6 EDX spectrum from the interface between the SiC particulate and the Al matrix.

precipitate (marked A) with a size less than 20 nm was observed. Since no additional diffraction spots were observed, it is believed that these precipitates are a kind of Guinier–Preston (GP) zone. Because the GP zones of the Mg_2Si sequence and Si sequence are needle-shaped and spherical, respectively [19, 20], the small GP zones observed must be GP zones of the Si sequence. A certain amount of dislocation has also been observed in the Al matrix. This is attributed to the difference of thermal expansion coefficient between the SiC particulate and the matrix [23, 24].

Fig. 10a is the morphology of another kind of spherical precipitate with a much larger size. It produces no SAD pattern. This suggests that it has an amorphous structure. Fig. 10b is the corresponding EDX spectrum indicating a chemical composition of $Al_9Si_9Ca_2$. Table III shows the results of calculation. Due to the influence of the matrix, the Al content in the phase is an approximate value.

3.4. The constituent phase

Fig. 11 shows the respective BF and DF images of a constituent phase with a size of 0.8 μm. Its morphology is rather like that of eutectic Si. The corresponding SAD patterns are given in Fig. 12. The

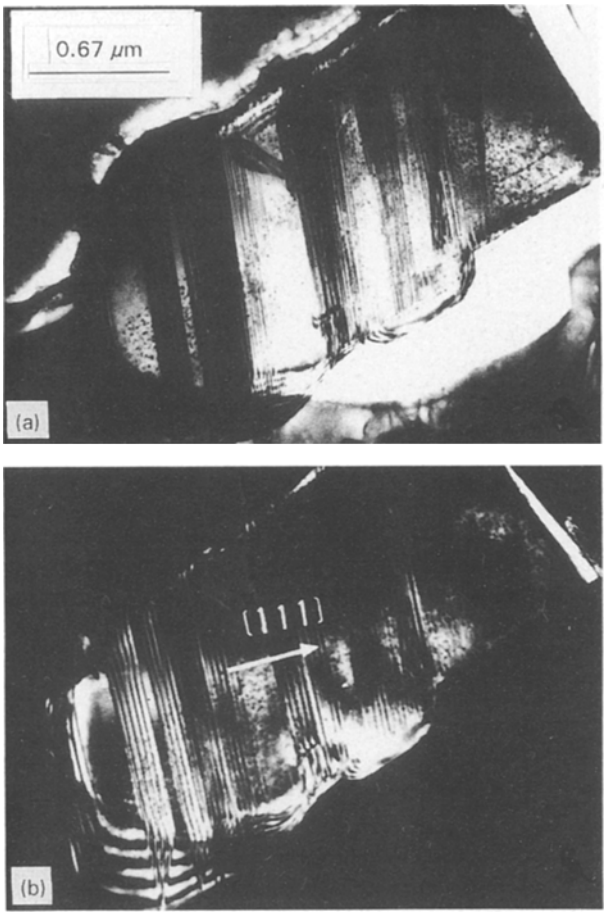

Figure 7 Morphology of eutectic Si: (a) BF, (b) DF.

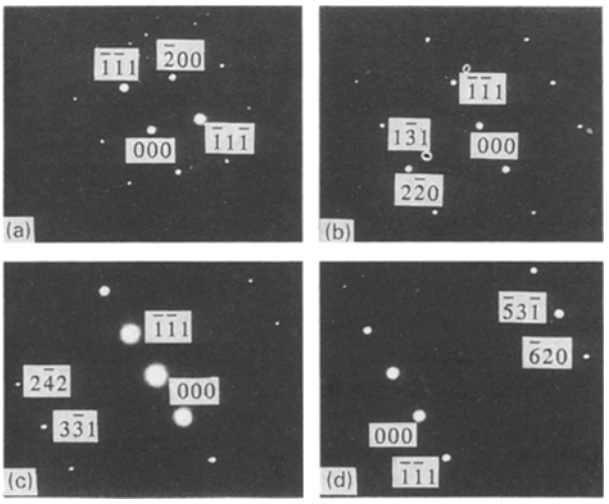

Figure 8 SAD patterns of eutectic Si in Fig. 7.

measured values for these SAD patterns are shown in Table IV.

Since the SAD patterns of Fig. 12 could not be interpreted by any one of the previous studies [16–18], we have to believe that it is a new constituent phase and have designated it as the J phase. It is then determined that the constituent phase has a C-face-centred orthorhombic crystal structure with $a = 0.680$ nm, $b = 1.170$ nm and $c = 0.826$ nm. Table V shows the results of calculation which correspond to the experimental results of Table IV.

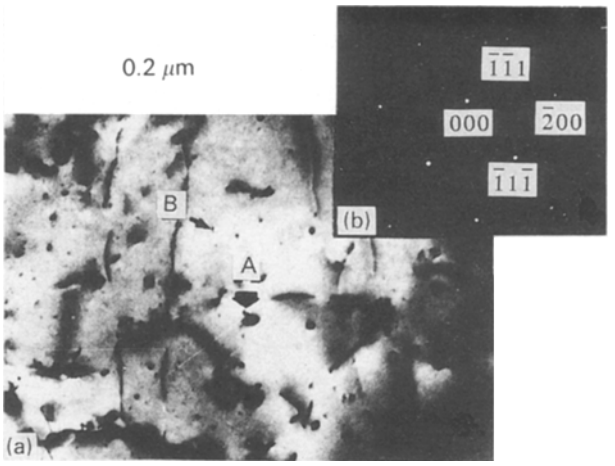

Figure 9 Morphology of GP zones of Si sequences and the corresponding SAD pattern.

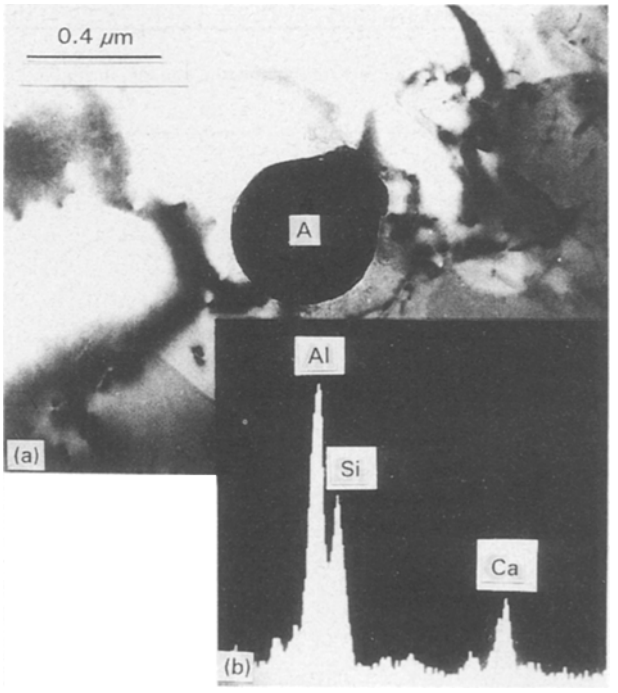

Figure 10 Morphology of amorphous $Al_xSi_9Ca_2$ phase and the corresponding EDX spectrum.

As before, the crystal structure of the J phase could also be verified through comparison of the calculated inter-angles between the reciprocal planes in Table V with the corresponding measured inter-angles between the SAD patterns in Fig. 12. The following shows the comparison; the results are satisfactory.

Fig. 12a ^ Fig. 12b = 19.51° [1 0 0] ^ [5 1 0] = 18.99°

Fig. 12b ^ Fig. 12c = 5.38° [5 1 0] ^ [4 1 0] = 4.29°

Fig. 12c ^ Fig. 12d = 6.09° [4 1 0] ^ [3 1 0] = 6.56°

Fig. 12d ^ Fig. 12a = 30.11° [3 1 0] ^ [1 0 0] = 29.84°

Fig. 13 is a schematic diagram of the indexed patterns. Fig. 13a, b, c and d correspond to Fig. 12a, b, c and d, respectively.

TABLE III Calculations from EDX spectrum of the amorphous phase in Fig. 10

Element	K ratio	Z	A	F	ZAF	wt %	at %
Si-K	0.075	0.985	5.997	0.998	5.894	44.44	45.54
Al-K	0.259	1.012	1.621	0.982	1.610	41.75	44.54
Ca-K	0.054	1.012	2.523	1.000	2.553	13.81	9.92

TABLE IV Measured values of SAD patterns in Fig. 12

Fig. No.	R_2/R_1	θ(°)	d_1 (nm)
12a	1.412	90.0	0.826
12b	3.710	90.0	0.826
12c	6.166	90.0	0.826
12d	2.432	90.0	0.826

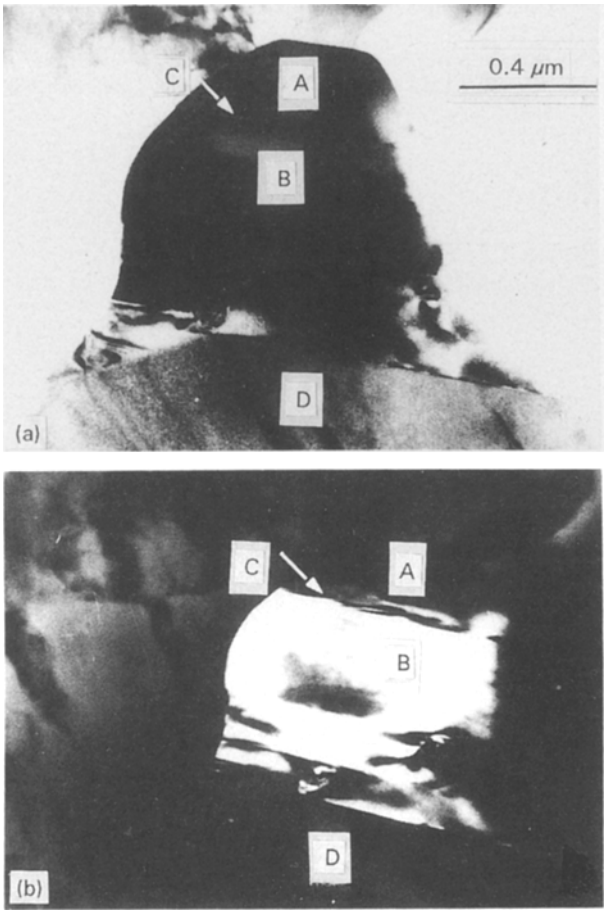

Figure 11 Morphology of J phase: (a) BF, (b) DF.

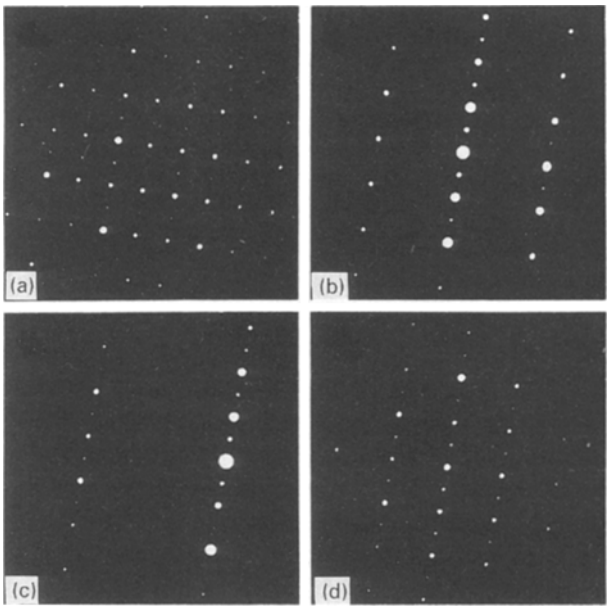

Figure 12 SAD patterns of J phase in Fig. 11.

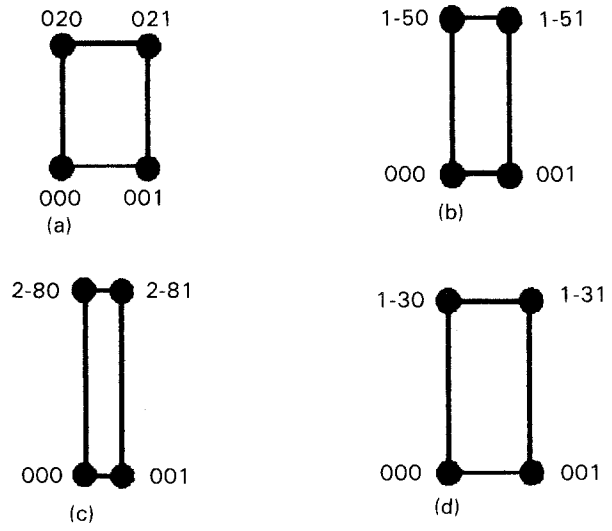

Figure 13 Indexed patterns corresponding to the SAD patterns in Fig. 12.

TABLE V Calculated values of SAD patterns in Fig. 12

Fig. No.	R_2/R_1	θ (°)	d_1 (nm)	$(h_1 k_1 l_1)$	$(h_2 k_2 l_2)$	$[U V W]$
12a	1.412	90.00	0.826	001	020	100
12b	3.734	90.00	0.826	001	1 − 50	510
12c	6.150	90.00	0.826	001	2 − 80	410
12d	2.442	90.00	0.826	001	1 − 30	310

4. Conclusions

1. The SiCp-reinforced A356 cast Al metal-matrix composite contains β-SiC, $(\beta + \gamma_2)$SiC composite, eutectic Si, GP zones of Si sequence, the J phase and a spherical-shape amorphous phase with chemical composition $Al_xSi_9Ca_2$.

2. The γ_2-SiC is a new variant of SiC. It is lath-like with a triclinic crystal structure having $a = 0.308$ nm,

$b = 0.305$ nm, $c = 1.262$ nm, $\alpha = 93.8°$, $\beta = 90.0°$ and $\gamma = 60.0°$.

3. The J phase is a newly discovered constituent phase. It is bulk-like with a C-face-centred orthorhombic crystal structure having $a = 0.680$ nm, $b = 1.170$ nm and $c = 0.826$ nm.

Acknowledgement

We thank the Chinese Science Foundation of Aeronautics for support.

References

1. J. D. H. ONNAY and H. M. ONDIK, "Crystal Data" (USA, 1973) p. H199.
2. X. G. NING, H. G. XU, H. Q. YE, J. ZHU, K. Y. HU, Y. X. LU and J. BI, *Phil. Mag. A* **63** (1990) 727.
3. LIU QING, WU KUN, L. GENG and C. K. YAO, *Mater. Sci. Eng.* **A130** (1990) 113.
4. S. R. NUTT, *J. Amer. Ceram. Soc.* **67** (1984) 428.
5. *Idem, ibid.* **71** (1988) 149.
6. ZHOU YANCHUN, CHANG XIN, ZHOU JING and XIA FEI, *Acta Metall. Sinica* **B4** (1991) 283.
7. Y. C. ZHOU, X. CHANG, J. ZHOU, F. XIA and C. H. SHIH, *Phil. Mag. Lett.* **63** (1991) 19.
8. R. L. MECHAN and R. B. BOLON, *J. Mater. Sci.* **14** (1979) 2471.
9. I. H. KAHN, *Metall. Trans.* **7A** (1982) 1281.
10. R. J. ARSHENAULT and C. S. PONDE, *Scripta Metall.* **18** (1984) 1131.
11. L. CAO, L. GENG, C. K. YAO and T. C. LEI, *ibid.* **23** (1989) 227.
12. M. STRANGWOOD, C. A. HIPPSLEY and J. J. LEWANDOWSKI, *ibid.* **24** (1990) 1483.
13. P. MAGUIN, J. T. MASON and R. TRIVEDI, *Acta Metall.* **39** (1991) 461.
14. LIU QING, ZHANG HU and LI QINGCHUN, *Scripta Metall.* **24** (1990) 1975.
15. M. SHANSUZZOHA and L. M. HOGAN, *Metallography* **22** (1989) 27.
16. ZHOU ZHAO, SONG SHIJIAN and XU YINGKUN, *Mater. Sci. Eng.* **A132** (1991) 83.
17. G. GUSTAFASSON, T. THORVALDSSON and G. L. DUNLOP, *Metall. Trans.* **17A** (1986) 45.
18. B. CLOSSET and J. E. GRUZLESKI, *ibid.* **13A** (1982) 945.
19. L. F. MONDOLFO, "Aluminium Alloys: Structure and Properties" (Butterworths, London, 1976) p. 566.
20. H. SUZUKI and M. KANNO, *J. Jap. Inst. Light Met.* **31** (1982) 277.
21. LI CHUNZHI and YAN MINGGAO, *Chinese J. Met. Sci. Tech.* **3** (1987) 27.
22. HUANG XIAOYING, "Transmission Electron Microscopy" (Shanghai Press of Science and Technology, Shanghai, 1987) p. 315.
23. H. RIBES and M. SUERY, *Scripta Metall.* **23** (1989) 705.
24. T. CHRISTMAN and S. SURESH, *Acta Metall.* **36** (1988) 1691.

Received 27 February
and accepted 10 December 1992